Astrometric and photometric initial mass functions from the UKIDSS Galactic Clusters Survey – III. Praesepe[*]

S. Boudreault,[1,2]† N. Lodieu,[1,2] N. R. Deacon[3] and N. C. Hambly[4]

[1]*Instituto de Astrofísica de Canarias (IAC), C/Vía Láctea s/n, E-38200 La Laguna, Tenerife, Spain*
[2]*Departamento de Astrofísica, Universidad de La Laguna (ULL), E-38205 La Laguna, Tenerife, Spain*
[3]*Max-Planck-Institute für Astronomie, Königstuhl 17, 69117 Heidelberg, Germany*
[4]*Scottish Universities P̃hysics Alliance (SUPA), Institute for Astronomy, School of Physics & Astronomy, University of Edinburgh, Royal Observatory, Blackford Hill, Edinburgh EH9 3HJ*

ABSTRACT

Over the past decades open clusters have been the subject of many studies. Such studies are crucial considering that the universality of the initial mass function is still a subject of current investigations. Praesepe is an interesting open cluster for the study of the stellar and substellar mass function (MF), considering its intermediate age and its nearby distance. Here we present the results of a wide-field, near-infrared study of Praesepe using the Data Release 9 of the United Kingdom Infrared Telescope Infrared Deep Sky Survey Galactic Clusters Survey. We obtained cluster candidates of Praesepe based on a 3σ astrometric and five-band photometric selection. We derived a binary frequency for Praesepe of 25.6 ± 3.0 per cent in the 0.2–0.45 $M_\odot$ mass range, 19.6 ± 3.0 per cent for 0.1–0.2 $M_\odot$ and 23.2 ± 5.6 per cent for 0.07–0.1 $M_\odot$. We also studied the variability of the cluster candidates of Praesepe, and we conclude that seven objects could be variable. We inferred the luminosity function of Praesepe in the Z and J bands and derived its MF. We observe that our determination of the MF of Praesepe differs from previous studies: while previous MFs present an increase from 0.6 to 0.1 $M_\odot$, our MF shows a decrease. We looked at the MF of Praesepe in two different regions of the cluster, i.e. within and beyond $1°\!.25$, and we observed that both regions present an MF which decrease to lower masses. We compared our results with the Hyades, the Pleiades and α Per MF in the mass range 0.072–0.6 $M_\odot$ and showed that the Praesepe MF is more similar to α Per although they are, respectively, of ages $\sim$85 and $\sim$600 Myr. Even though of similar age, the Praesepe remains different than the Hyades, with a decrease in the MF of only $\sim$0.2 dex from 0.6 down to 0.1 $M_\odot$, compared to $\sim$1 dex for the Hyades.

Key words: techniques: photometric – brown dwarfs – stars: low-mass – stars: luminosity function, mass function – open clusters and associations: individual: Praesepe – infrared: stars.

1 INTRODUCTION

Over the past decades, open clusters have been the subject of many studies (e.g. Bastian, Covey & Meyer 2010 and references therein). Such studies have brought new insights into brown dwarf (BD) formation (e.g. Kumar & Schmeja 2007; Boudreault & Bailer-Jones 2009; Béjar et al. 2011), on the discovery of young L and T dwarfs and free-floating planets (e.g. Bouvier et al. 2008; Lodieu

et al. 2008; Peña Ramírez et al. 2008; Zapatero Osorio et al. 2008; Bihain et al. 2009; Lucas et al. 2010; Quanz et al. 2010) and on our understanding of the stellar/substellar mass function (MF; see the review by Bastian et al. 2010) and their populations in the Galactic field and in open clusters (see the review by Chabrier 2003). Such studies are crucial considering that the universality of the initial mass function (IMF) is still a subject of current investigations (e.g. Kroupa 2002; Covey, Bastian & Meyer 2011; Myers et al. 2011; Leigh et al. 2012; Marks & Kroupa 2012). Most works on the substellar MF have focused on young open clusters with ages less than $\sim$150 Myr. This is partly because BDs are bright when they are young, thus aiding the detection of the least massive objects. However, the extension of MF studies to older clusters is vital as it allows us to study the intrinsic evolution of BDs and how the stellar and substellar population itself evolves.

Praesepe (M44, NGC 2632, RA $= 8^{\mathrm{h}}\,40^{\mathrm{m}}4$, Dec. $= +19°41'$) is an interesting open cluster to study the MF in the stellar and substellar regimes, considering its age ($\tau = 590^{+150}_{-120}$ Myr; Fossati et al. 2008) and its distance [$(m - M)_0 = 6.30 \pm 0.07$ mag, $d = 181.97^{+5.96}_{-5.77}$ pc; van Leeuwen 2009], its known proper motion ($\mu_\alpha = -35.81 \pm 0.29$ mas yr^{-1} and $\mu_\delta = -12.85 \pm 0.24$ mas yr^{-1}; van Leeuwen 2009) and the low extinction towards this cluster [$E(B - V) = 0.027 \pm 0.004$; Taylor 2006], while determinations of the metallicity of Praesepe go from solar type with [Fe/H] $= 0.038 \pm 0.039$ dex (Friel & Boesgaard 1992) to slightly metal rich with [Fe/H] $= 0.27 \pm 0.10$ dex (Pace, Pasquini & Franois 2008). So far, several surveys for stellar and substellar objects in the open cluster Praesepe have been performed (e.g. Jones & Cudworth 1983; Hodgkin et al. 1999; Baker et al. 2010). Some surveys have the advantage of covering a large area and using proper motions, but are rather shallow (e.g. Hambly et al. 1995; Kraus & Hillenbrand 2007), while other surveys used deep photometry, but lacked wide areal coverage (e.g. González-García et al. 2006; Boudreault et al. 2010; Wang et al. 2011).

The UKIRT Infrared Deep Sky Survey (UKIDSS; Lawrence et al. 2007) is a deep large-scale infrared survey conducted with the Wide-Field Camera (WFCAM; Casali et al. 2007) on UKIRT (Mauna Kea, Hawaii). The survey is subdivided into five components: the Large Area Survey, the Galactic Clusters Survey (hereafter GCS), the Galactic plane Survey, the Deep Extragalactic Survey and the Ultra-Deep Survey. The GCS aims at covering $\sim$1000 square degrees in 10 star-forming regions and open clusters down to $K = 18.4$ mag at two epochs. The main scientific driver of the survey is to study the IMF and its dependence on the environment in the substellar regime using a homogeneous set of low-mass stars and BDs over large areas in several regions. The UKIDSS GCS is, therefore, a perfect tool to study the open cluster Praesepe, considering the large coverage from the UKIDSS Data Release 9 (DR9) with its relative deep photometry spanning from $J \sim 10.9$ mag (i.e. $\sim 0.7\,\mathrm{M}_\odot$) down to $J \sim 19.3$ mag (i.e. $\sim 55\,\mathrm{M_{Jup}}$), combined with astrometric information.

Here we present the results of a wide-field near-infrared study of the Praesepe cluster using the DR9 of the UKIDSS GCS. The paper is structured as follows. First, we present the data set used in our analysis (Section 2), followed by a cross-match with previous surveys (Section 3). Then, we extract the new stellar and substellar members in Praesepe based on our selection criteria (Section 4). We discuss the level of contamination (Section 5), the multiplicity of low-mass Praesepe members (Section 6) and the variability of our cluster candidates (Section 7). Finally, we derive the luminosity function (LF) and MF of Praesepe (Section 8).

2 THE PHOTOMETRIC AND ASTROMETRIC SAMPLE

The UKIDSS GCS DR9 covers $\sim$36 square degrees observed in five passbands ($ZYJHK$; Hewett et al. 2006) in the Praesepe cluster over a region defined by RA $= 126°$–$134°$ and Dec. $= 16°\!.5$–$23°\!.0$. Unfortunately, we are missing a region of $\sim$0.585 square degrees in the central region of Praesepe, delineated by (RA, Dec.) from (130°.37, 19°.3) to (131°.2, 19°.75) and (130°.37, 19°.75) to (130°.84, 20°.2) (Fig. 1).

We selected all good quality point sources in Praesepe detected in *JHK* with no constraint on detection in Z, Y and *K2* (second epoch *K* band). We imposed a selection on point sources only in *JHK* and pushed the completeness towards the faint end by insisting on the CLASSSTAT parameters which represent the roundness of an image (i.e. $-3 <$ CLASSSTAT $< +3$). The Structured Query Lan-
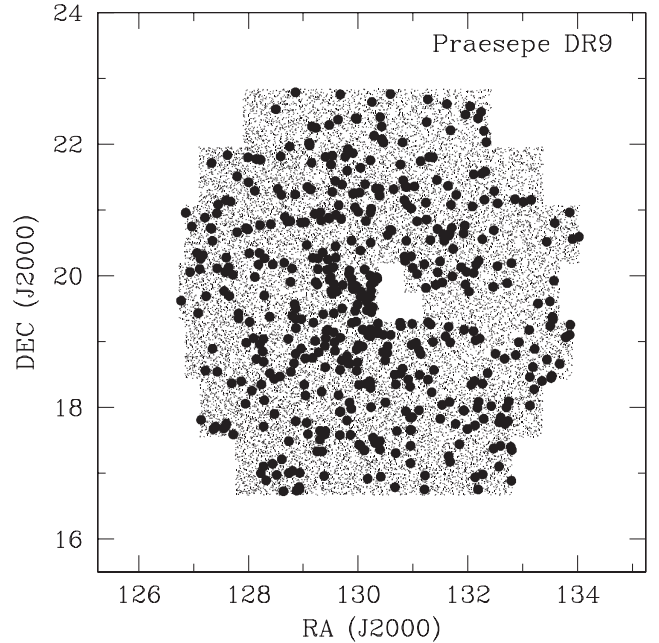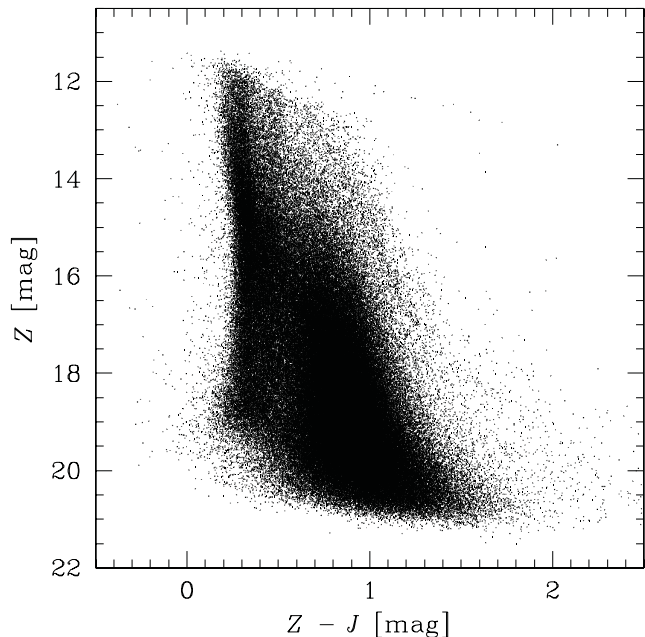

Figure 1. All detected objects towards Praesepe as released by the UKIDSS GCS DR9 (small black dots). For clarity, only 1 of 10 objects are plotted. We also show the objects which are recovered in our astrometric and photometric selection (larger black dots, see Section 4). The missing region at the centre is due to poor quality images that were discarded during the quality control process of UKIDSS.
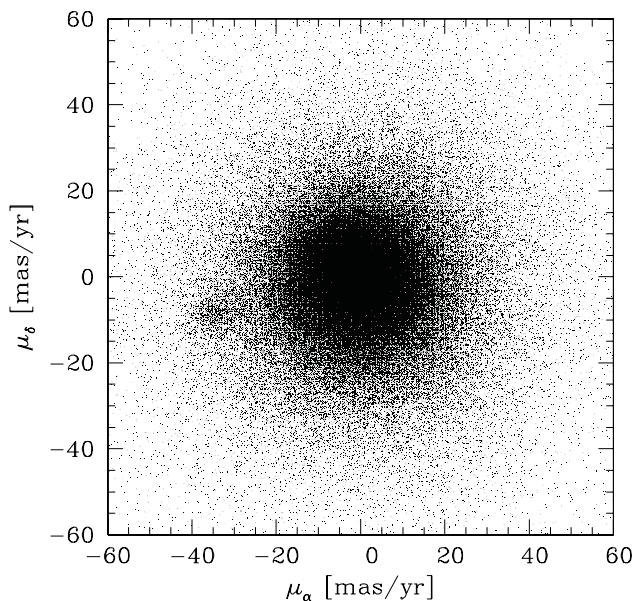
guage (SQL) query used to select sources along the line of sight of the Praesepe is identical to the query used for the Pleiades (Lodieu, Deacon & Hambly 2012). The SQL query includes the cross-match with Two Micron All Sky Survey (2MASS; Cutri et al. 2003; Skrutskie et al. 2006) to compute proper motions for all sources brighter than the 2MASS 5σ completeness limit at $J = 15.8$ mag as well as the selection of proper motion information from that newly available in UKIDSS DR9. We used the GCS proper motion measurements in this work as they are more accurate due to the homogeneous coverage, completeness and spatial resolution of the GCS. We limited our selection to sources fainter than $Z = 11.7$, $Y = 11.8$, $J = 10.9$, $H = 11.4$, $K1 = 10.0$ and $K2 = 10.4$ mag to avoid saturation. The completeness limits, taken as the magnitude where the straight line fitting the shape of the number of sources as a function of magnitudes falls off, are $Z = 20.4$, $Y = 20.0$, $J = 19.3$, $H = 18.7$, $K1 = 17.9$ and $K2 = 18.4$ mag. (The method for deriving the detection limit is presented in Lodieu et al. 2009.)

The query returned 218 141 sources with $J = 10.9$–21.2 mag over 36 square degrees towards Praesepe. The full GCS DR9 coverage is displayed in Fig. 1. The resulting ($Z - J$, Z) colour–magnitude diagram (CMD) is shown in Fig. 2.

Proper motion measurements are available in the WFCAM Science Archive for UKIDSS data releases from the DR9 for all the wide/shallow survey with multiple epoch coverage in each field, including the GCS. The details of the procedure to derive the relative proper motions is described in detail in Collins & Hambly (2012) and a summary is given in Lodieu et al. (2012). The proper motion vector point diagram for all sources detected towards Praesepe is presented in Fig. 3.

Figure 2. CMD of Z versus $Z - J$ of all detected objects towards Praesepe from the UKIDSS GCS DR9. The cluster sequence of Praesepe is clearly visible between $(Z - J, Z) \sim (0.6, 12.5)$ and $(Z - J, Z) \sim (1.3, 17)$.

Table 1. Updated membership of the Praesepe member candidates published in the literature and recovered by the GCS DR9. Papers dedicated to Praesepe over the past two decades are ordered by year. References are Jones & Cudworth (1983), Hambly et al. (1995), Hodgkin et al. (1999), González-García et al. (2006), Kraus & Hillenbrand (2007), Baker et al. (2010), Boudreault et al. (2010) and Wang et al. (2011). Column 2 gives the numbers of cluster member candidates published in the reference given in column 1. Column 3 gives the numbers of sources recovered in GCS DR9. Column 4 gives the percentages of sources recovered in the GCS DR9. Columns 5 and 6 give the number of members and non-members based on our photometric and astrometric analysis, respectively.

Survey	All	DR9	Per cent	Member	NM
Jones & Cudworth (1983)	206	106	66.5	49	57
Hambly et al. (1995)	515	383	74.4	323	60
Hodgkin et al. (1999)	17	10	58.8	6	4
González-García et al. (2006)	20	14	70.0	1	13
Kraus & Hillenbrand (2007)	1130	711	62.9	654	57
Baker et al. (2010)	147	146	99.3	125	21
Boudreault et al. (2010)	150	100	66.7	37	61
Wang et al. (2011)	59	29	49.2	7	22

In Table 1, we present the numbers of cluster candidates published by each study (All) and the corresponding numbers of cluster candidates retrieved by the GCS (DR9). We also present in this table the number of objects recovered in our astrometric and photometric selections (see Section 4).

For some works (e.g. Jones & Cudworth 1983; Hodgkin et al. 1999), the ratios of Praesepe member candidates published in the literature and recovered by the GCS DR9 are low (i.e. 51.5 and 58.8 per cent, respectively). These older works had shallow photometry and most of their candidates are saturated in the GCS DR9. Other works have large coverage beyond the area of the GCS DR9, with more than 30 and 300 square degrees for Hambly et al. (1995) and Kraus & Hillenbrand (2007), respectively. As for the cluster candidates from previous deep surveys (i.e. González-García et al. 2006; Boudreault et al. 2010; Wang et al. 2011), the objects not recovered are either too faint for UKIDSS GCS or they are in the central area not covered (see Fig. 1). Finally, all but one (not detected in the second epoch of the K-band observations) object from Baker et al. (2010) are recovered, since this work was based on an earlier release of the UKIDSS GCS.
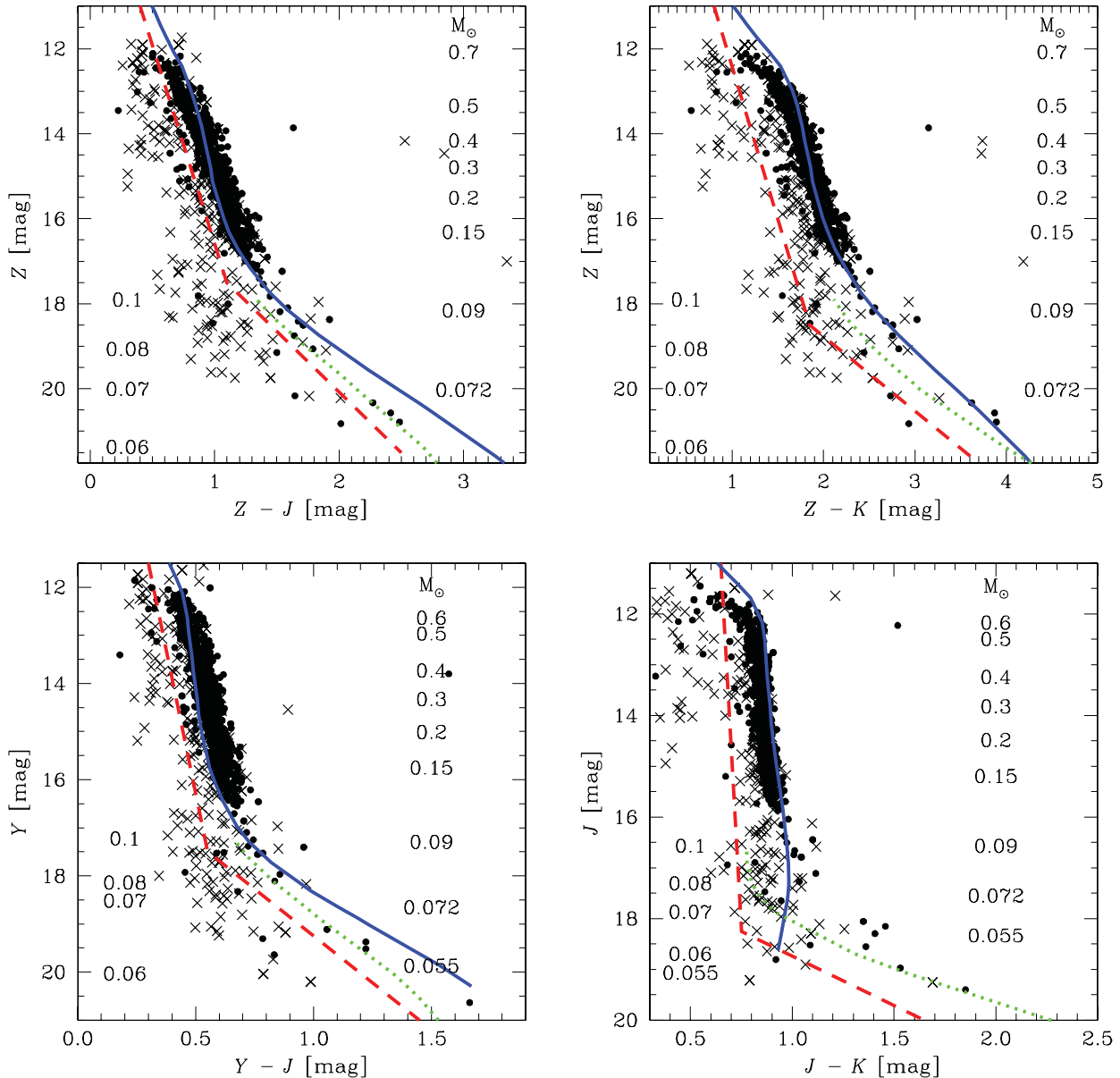
In Fig. 4, we present in four CMDs all Praesepe member candidates published in the literature and recovered by the GCS DR9. We use these previous cluster candidates with proper motions consistent with Praesepe membership (and those classified as proper motion non-members) to define selection lines which will be used for our photometric selection (see Section 4).

4 NEW STELLAR AND SUBSTELLAR MEMBERS IN THE PRAESEPE

The selection used in this work and presented in Sections 4.1 and 4.2 is identical to our studies of the Pleiades (Lodieu et al. 2012) and α Per (Lodieu et al., in preparation) clusters. The main scientific goals of these studies are to perform a homogeneous analysis of the LF and MF of the Pleiades, α Per and Praesepe.

4.1 Astrometric selection

First we performed a selection based on the proper motion of Praesepe. The proper motion values of van Leeuwen (2009) are the

Figure 3. Proper motion diagram of all detected objects towards Praesepe from the UKIDSS GCS DR9. The position of Praesepe is clearly visible at $\mu_\alpha = -34.17 \pm 2.74 \, \text{mas yr}^{-1}$ and $\mu_\delta = -7.36 \pm 4.17 \, \text{mas yr}^{-1}$.

3 CROSS-MATCH WITH PREVIOUS SURVEYS

We compiled a list of member candidates of Preasepe published from previous studies in Jones & Cudworth (1983), Hambly et al. (1995), Hodgkin et al. (1999), González-García et al. (2006), Kraus & Hillenbrand (2007), Baker et al. (2010), Boudreault et al. (2010) and Wang et al. (2011). We matched these previously known members with the 218 141 sources from UKIDSS GCS DR9 towards Praesepe. Only those members with positions that are within 3 arcsec of the location of each object in these previous catalogues are included in our sample.

Figure 4. CMDs showing previously reported members of Praesepe recovered in UKIDSS DR9 GCS. Previously known members are taken from Jones & Cudworth (1983), Hambly et al. (1995), Hodgkin et al. (1999), González-García et al. (2006), Kraus & Hillenbrand (2007), Baker et al. (2010), Boudreault et al. (2010) and Wang et al. (2011). The filled dots are the objects which have a proper motion consistent with Praesepe membership (3σ astrometric selection), while the objects presented with the crosses do not. The NextGen isochrones are the solid blue lines with masses on the right, while the DUSTY isochrones are the dotted green lines with masses on the left. The dashed red lines represent our photometric selection criteria in each diagram as detailed in Section 4.

absolute proper motion measurements obtained with *Hipparcos*. Here, the proper motion values from UKIDSS are relative to a reference frame defined by the faintest, most numerous objects detected in each frame. The position of the cluster in the *relative* proper motion diagram of Fig. 3 is $\mu_\alpha = -34.17 \pm 2.74\,\mathrm{mas\,yr^{-1}}$ and $\mu_\delta = -7.36 \pm 4.17\,\mathrm{mas\,yr^{-1}}$.[1] We select all objects within $3\sigma_{\mu_\alpha}$ of μ_α and within $3\sigma_{\mu_\delta}$ of μ_δ, where $3\sigma_{\mu_\alpha}$ and $3\sigma_{\mu_\delta}$ are the errors on the measurement of μ_α and μ_δ of each source in the UKIDSS GCS DR9, respectively. All the objects selected astrometrically within

3σ are presented in a CMD of Z versus $Z - J$ in Fig. 5. From 218 141 sources detected in the UKIDSS GCS DR9 towards Praesepe, 33 854 objects are retrieved from our 3σ astrometric selection (15.5 per cent).

4.2 Photometric selection

We used the selection lines plotted in the CMDs of Fig. 4 to perform the photometric selection of our cluster candidates. These lines were chosen based on the position of previously reported Praesepe members recovered in UKIDSS GCS DR9 and by our astrometric selection. These lines are $\sim 2.5\sigma$ bluer than the location of the cluster sequence, where the value of σ is the distribution in colour

---

[1] We simply used the median of the distribution in μ_α (between -40 and $-30\,\mathrm{mas\,yr^{-1}}$) and μ_δ (between -15 and $-2\,\mathrm{mas\,yr^{-1}}$) for all objects within $J < 17\,\mathrm{mag}$.
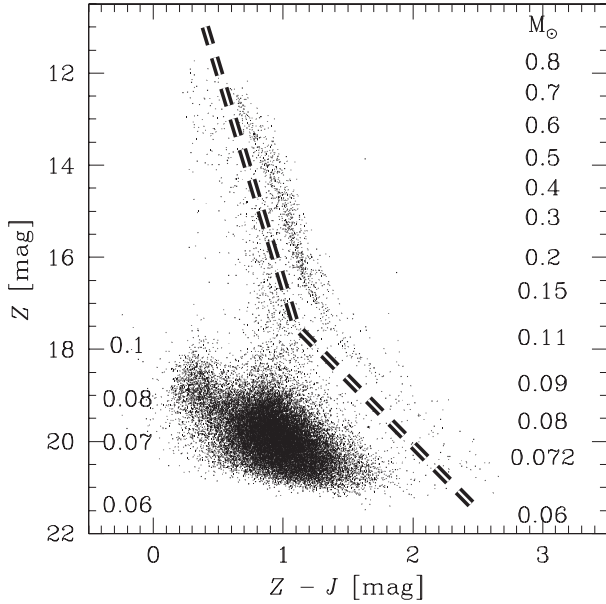
Figure 5. CMDs of Z versus $Z - J$ of all detected objects towards Praesepe from the UKIDSS GCS DR9 with a proper motion within 3σ of the cluster's mean proper motion. The masses corresponding to the Z magnitudes are given on the right (using a NextGen isochrone) and on the left (using a DUSTY isochrone). The black and white dashed lines are our photometric selection criteria (see Fig. 4).

of the cluster sequence in four different bins of magnitude. The photometric criteria were defined as follows:

(i) candidates should be detected in the $ZYJHK$ bands;

(ii) candidates should lie above the lines defined by $(Z - J, Z) = (0.4, 11)$ and $(1.1, 17.5)$, and by $(Z - J, Z) = (1.1, 17.5)$ and $(2.5, 21.5)$;

(iii) candidates should lie above the lines defined by $(Z - K, Z) = (0.8, 11)$ and $(1.85, 18.5)$, and by $(Z - K, Z) = (1.85, 18.5)$ and $(3.7, 21.75)$;

(iv) candidates should lie above the lines defined by $(Y - J, Y) = (0.3, 11.5)$ and $(0.55, 17.5)$, and by $(Y - J, Y) = (0.55, 17.5)$ and $(1.45, 21)$;

(v) candidates should lie above the lines defined by $(J - K, J) = (0.65, 11)$ and $(0.75, 18.25)$, and by $(J - K, J) = (0.75, 18.25)$ and $(1.65, 20)$.

This is presented in Fig. 6, where we show the same four CMDs in Fig. 4 and the objects recovered by our astrometric selection. We also present the previously reported members of Praesepe recovered in UKIDSS DR9 GCS.

From 33 854 objects from our astrometric selection, 1116 are retrieved from our photometric selection (3.3 per cent). This final selection gives us the objects which will be used for our following analysis. Our cluster candidates are listed in Tables 2 and 3.

4.3 Search for lower mass members

Here we search for fainter and coolsubstellar members of the Praesepe by trawling our selection first for stars having no Z-band detection, and secondly for stars having no Z- and Y-band detections.

4.3.1 Search for lower mass members detected in YJHK

To extend the cluster sequence to fainter objects, we searched for Praesepe candidate members undetected in Z. We imposed similar photometric and astrometric criteria as in Sections 4.1 and 4.2 but without detection in Z as follows:

(i) candidates should not be detected in the Z band;

(ii) candidates should have a proper motion within 3σ of the cluster's mean proper motion;

(iii) candidates should have $Y \geq 18$ and $J \leq 18.8$ mag;

(iv) candidates should lie above the lines defined by $(Y - J, Y) = (0.3, 11.5)$ and $(0.55, 17.5)$, and by $(Y - J, Y) = (0.55, 17.5)$ and $(1.45, 21)$;

(v) candidates should lie above the lines defined by $(J - K, J) = (0.65, 11)$ and $(0.75, 18.25)$, and by $(J - K, J) = (0.75, 18.25)$ and $(1.65, 20)$.

Out of 17 objects selected based on astrometry and without detections in Z, 16 are selected based on the colour cut above (94.2 per cent). All 16 objects have an existing image in the Z band in the UKIDSS GCS DR9 data base. A list of these 16 objects is presented in Table 4.

4.3.2 Search for lower mass members detected in JHK

We repeated the procedure described above looking for Z and Y non-detections. We applied the following criteria:

(i) candidates should not be detected in Z and Y bands;

(ii) candidates should have a proper motion within 3σ of the cluster's mean proper motion;

(iii) candidates should have $J \geq 18$ and $J \leq 18.8$ mag;

(iv) candidates should lie above the lines defined by $(J - K, J) = (0.65, 11)$ and $(0.75, 18.25)$, and by $(J - K, J) = (0.75, 18.25)$ and $(1.65, 20)$.

Out of 71 objects selected based on astrometry and without detections in Z and Y, 17 are selected based on the colour cut above (23.9 per cent), but only two objects have an existing image in the Z and Y bands in the UKIDSS GCS DR9 data base and remain undetected. These two objects are listed in Table 4.

4.4 Formal membership probabilities

As a check on our photometric and astrometric selection, we calculate formal membership probabilities based on the analysis of Deacon & Hambly (2004). This uses a method similar to Sanders (1971) who first proposed calculating membership probabilities from proper motions and to Hambly et al. (1995) who built on this method. In this method, the proper motion vector point diagram is rotated so that the cluster lies on the y' axis,
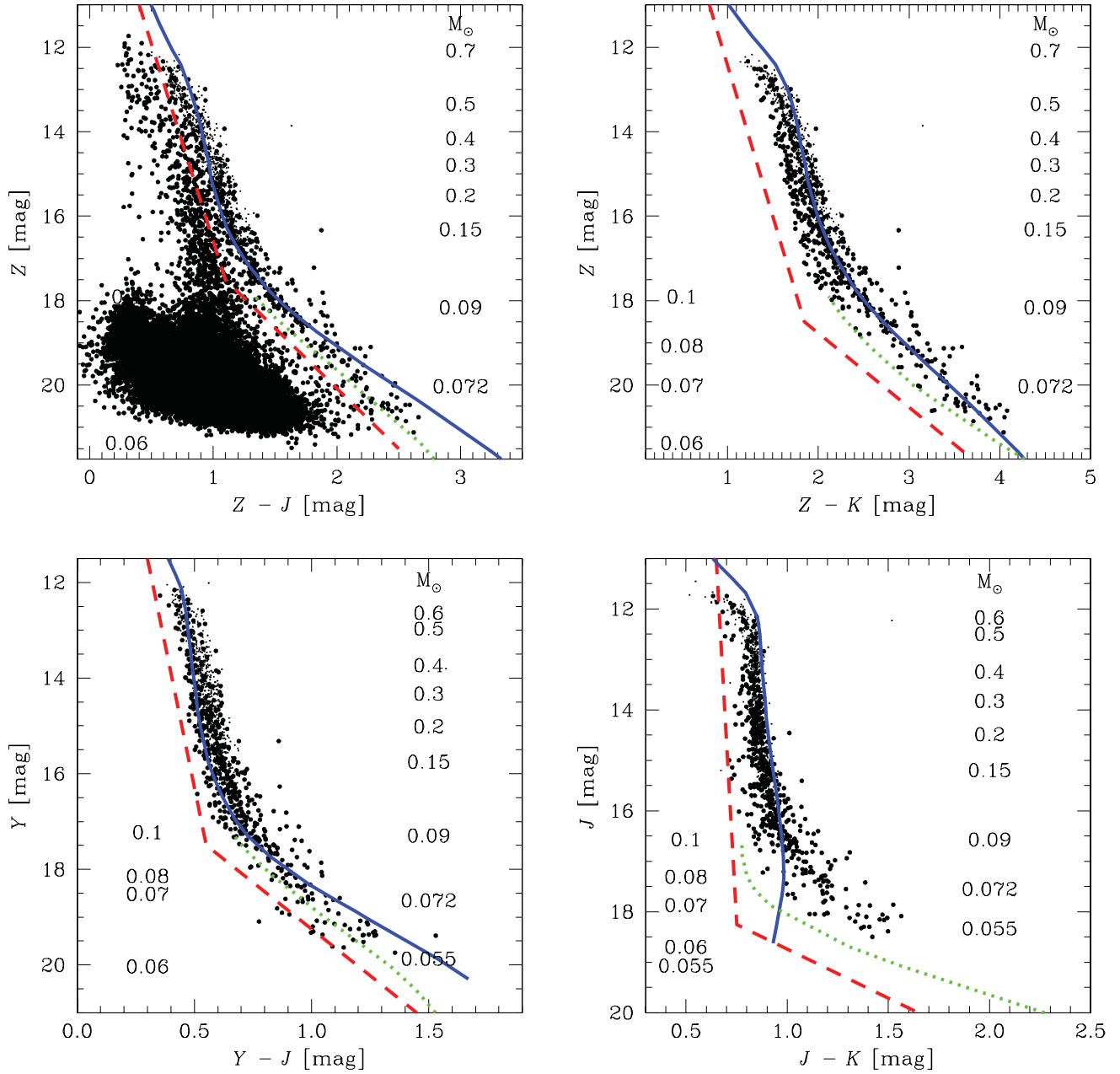
$$x' = \cos(-0.55\pi)x - \sin(-0.55\pi)y \tag{1}$$

$$y' = \cos(-0.55\pi)y + \sin(-0.55\pi)x, \tag{2}$$

and the distribution of proper motions in this vector point diagram is defined as

$$\Phi = f\Phi_f + (1 - f)\Phi c, \tag{3}$$

where Φ_f is the field star distribution defined as

$$\Phi_f = \frac{c_0}{\sqrt{(2\pi)}\Sigma_x}\exp\left(-\frac{\mu_y}{\tau} - \frac{(\mu_x - \mu_{xf})^2}{2\Sigma_x^2}\right). \tag{4}$$

Figure 6. Same as Fig. 4, showing previously reported members of Praesepe (small dots) recovered in UKIDSS DR9 GCS, and for which the proper motion is consistent with Praesepe membership. The larger dots are the objects for the UKIDSS DR9 GCS, but not reported before in the literature as cluster members. From one panel to the other, we only keep the objects redder than the red dashed lines, starting from Z versus $Z - J$ (top-left), followed by Z versus $Z - K$, to Y versus $Y - J$ and finally with J versus $J - K$.

Table 2. Praesepe member candidates based on our astrometric and photometric selection. Here we present the photometry and the astrometry of the candidates. The nomenclature used to identify the objects in this table is UGCS JHHMMSS.SS $\pm$ DDMMDD.D. Therefore, the first object in the table is UGCS J084644.83+221246.3. Table 2 is published in its entirety as supporting information with the electronic version of the journal. A fraction is shown here for guidance regarding its form and content.

RA (h m s)	Dec. (° ′ ″)	Z (mag)	Y (mag)	J (mag)	H (mag)	$K1$ (mag)	$K2$ (mag)	$\mu_\alpha \cos \delta$ (mas yr^{-1})	μ_δ (mas yr^{-1})
8:46:44.83	+22:12:46.3	16.914 ± 0.011	16.449 ± 0.009	15.865 ± 0.009	15.310 ± 0.009	15.024 ± 0.012	15.029 ± 0.006	−26.85 ± 3.54	−16.99 ± 3.54
8:43:15.16	+22:01:47.2	16.005 ± 0.006	15.546 ± 0.005	15.024 ± 0.005	14.427 ± 0.005	14.143 ± 0.005	14.162 ± 0.003	−29.28 ± 3.55	−3.86 ± 3.55
...	...	...	...	...	...	...	...	...	...
8:34:04.31	+16:58:24.7	15.394 ± 0.005	14.889 ± 0.004	14.321 ± 0.004	13.757 ± 0.003	13.455 ± 0.003	13.454 ± 0.002	−31.56 ± 3.45	2.76 ± 3.45
8:37:31.99	+16:57:35.7	14.978 ± 0.004	14.522 ± 0.003	13.905 ± 0.003	13.356 ± 0.002	13.052 ± 0.002	13.051 ± 0.002	−34.85 ± 3.45	−3.12 ± 3.45

Table 3. Praesepe member candidates based on our astrometric and photometric selection. Here we present the physical parameters of the candidates, i.e. mass and effective temperature (T_{eff}). The nomenclature used to identify the objects in this table is UGCS JHHMMSS.SS ± DDMMDD.D. Therefore, the first object in the table is UGCS J084644.83+221246.3. Table 3 is published in its entirety as supporting information with the electronic version of the journal. A fraction is shown here for guidance regarding its form and content.

RA (h m s)	Dec. (° ′ ″)	Mass (M$_\odot$)	T_{eff} (K)
8:46:44.83	+22:12:46.3	0.132 ± 0.005	3062 ± 125
8:43:15.16	+22:01:47.2	0.198 ± 0.013	3286 ± 217
...	...	...	...
8:34:04.31	+16:58:24.7	0.269 ± 0.006	3397 ± 74
8:37:31.99	+16:57:35.7	0.336 ± 0.013	3465 ± 138

Put simply the field population is modelled as an exponential in the y direction with scalelength τ, a Gaussian in the x' direction with mean μ_{xf} and standard deviation Σ_x and has normalization c_0. Φ_c is the cluster distribution:

$$\Phi_c = \frac{1}{2\pi\sigma^2}\exp-\frac{(\mu_x - \mu_{xc})^2 + (\mu_y - \mu_{yc})^2}{2\sigma^2}. \quad (5)$$

The cluster is fitted with a bivariant Gaussian with a single standard deviation (σ) centred on μ_{xc} and μ_{yc}. The membership probability is defined as

$$p = \frac{\Phi_c}{\Phi}. \quad (6)$$

In Deacon & Hambly (2004) and Lodieu et al. (2007), we allowed all our parameters to be freely fitted by a maximum likelihood method. However, here we take the approach taken in Lodieu et al. (2012) where the standard deviation of the cluster proper motions is fixed to be the proper motion measurement errors calculated in the appropriate magnitude bin.

The input list for the fitting procedure had the same source quality parameter cuts as listed in Section 2 with a single colour cut being applied,

(i) $Z < 7 \times (Z - J) + 9.5$ and $Z < 18.6$;
(ii) $Z < 3 \times (Z - J) + 14$ and $Z > 18.6$.

The fitted parameters for each brightness range are shown in Table 5. Note that the cluster position appears to migrate in the last fitted bin. This is likely not due to any real variation in the cluster proper motion but to the fitting procedure becoming unreliable for the faintest objects.

Table 6 contains a truncated list of high-priority ($p > 0.5$) candidates; the full list is available in electronic form (see the supporting information). Using the probabilistic analysis, we obtained a total of 1015 candidates with a membership probability higher than 50 per cent, comparable to the 1116 cluster candidates based on a photometric and astrometric selection. These objects are shown in Fig. 8 (right-hand panel) in the CMD of K versus $Z - K$ with all GCS point sources towards Praesepe.

5 ESTIMATION OF CONTAMINATION

The number density of field objects in our final list of candidates as a function of mass was obtained in a similar way as in Jeffries et al. (2004). We obtained the radial profile of our cluster candidates in three mass ranges: above 0.4 M$_\odot$, between 0.15 and 0.4 M$_\odot$ and below 0.15 M$_\odot$ (Fig. 7).

However, we must consider the first and last two data points with caution, as we are not complete in coverage within 1° and beyond 3°. Therefore, we are not complete at the tidal radius of Praesepe at 3°.5 ± 0°.1 (11.5 ± 0.3 pc; Kraus & Hillenbrand 2007) and not within its core radius at 1°.1 ± 0°.1 (3.5 ± 0.3 pc; Adams et al. 2002).

Therefore, we only use the bins between 2°.5 and 3° at each mass range to obtain an upper limit of contamination. This gives 1.27 objects per square degree for candidates with masses above 0.4 M$_\odot$, 3.70 between 0.15 and 0.4 M$_\odot$, and 2.08 objects per square degree

Table 4. Praesepe member candidates based on our astrometric and photometric selection using *YJHK* photometry (top lines) and using *JHK* photometry (last two lines). The nomenclature used to identify the objects in this table is UGCS JHHMMSS.SS ± DDMMDD.D. Therefore, the first object in the table is UGCS J084322.72+222646.6.

RA (h m s)	Dec. (° ′ ″)	Z (mag)	Y (mag)	J (mag)	H (mag)	K1 (mag)	K2 (mag)	$\mu_\alpha \cos\delta$ (mas yr^{-1})	μ_δ (mas yr^{-1})
8:43:22.72	+22:26:46.6	–	19.734 ± 0.123	18.154 ± 0.049	17.377 ± 0.062	16.630 ± 0.049	16.641 ± 0.029	−34.55 ± 5.91	−16.26 ± 5.91
8:45:07.82	+21:17:29.2	–	19.665 ± 0.146	18.358 ± 0.082	17.770 ± 0.063	17.041 ± 0.058	17.041 ± 0.041	−11.85 ± 7.63	−1.27 ± 7.63
8:40:20.81	+20:05:21.4	–	19.310 ± 0.076	18.241 ± 0.049	17.637 ± 0.072	16.966 ± 0.072	16.898 ± 0.033	−43.70 ± 5.78	−9.07 ± 5.78
8:37:15.19	+20:09:51.2	–	19.314 ± 0.076	18.097 ± 0.047	17.293 ± 0.039	16.553 ± 0.049	16.560 ± 0.025	−34.20 ± 5.97	1.55 ± 5.97
8:36:36.89	+20:07:00.7	–	19.269 ± 0.072	18.225 ± 0.053	17.433 ± 0.044	16.717 ± 0.054	16.727 ± 0.029	−29.03 ± 6.38	−8.23 ± 6.38
8:38:03.30	+19:47:15.0	–	19.881 ± 0.147	18.333 ± 0.068	17.403 ± 0.043	16.720 ± 0.049	16.725 ± 0.031	−31.72 ± 8.39	7.77 ± 8.39
8:45:47.32	+20:05:25.8	–	19.686 ± 0.117	18.504 ± 0.076	17.848 ± 0.069	17.534 ± 0.110	17.570 ± 0.068	−13.04 ± 8.35	−27.58 ± 8.35
8:34:22.13	+19:54:38.7	–	20.011 ± 0.161	18.623 ± 0.087	18.104 ± 0.094	17.560 ± 0.124	17.536 ± 0.068	−28.77 ± 10.31	−34.87 ± 10.31
8:39:22.81	+19:40:37.1	–	19.743 ± 0.113	18.472 ± 0.066	17.751 ± 0.071	17.050 ± 0.068	17.123 ± 0.039	−42.70 ± 6.02	−2.48 ± 6.02
8:39:01.37	+20:35:04.1	–	19.735 ± 0.111	18.546 ± 0.053	17.882 ± 0.071	17.286 ± 0.070	17.280 ± 0.051	−38.44 ± 6.47	−4.31 ± 6.47
8:38:05.45	+19:23:27.7	–	19.484 ± 0.095	18.246 ± 0.057	17.510 ± 0.045	16.993 ± 0.057	16.882 ± 0.032	−39.10 ± 8.34	−14.61 ± 8.34
8:47:35.00	+17:49:53.0	–	19.925 ± 0.149	18.602 ± 0.099	17.854 ± 0.065	17.409 ± 0.085	17.523 ± 0.060	−21.59 ± 11.13	−14.85 ± 11.13
8:44:25.06	+17:50:52.9	–	19.743 ± 0.124	18.418 ± 0.085	17.799 ± 0.063	16.883 ± 0.052	16.930 ± 0.035	−28.17 ± 6.92	8.40 ± 6.92
8:54:12.81	+18:26:11.7	–	19.825 ± 0.146	18.567 ± 0.075	17.943 ± 0.072	17.377 ± 0.099	17.300 ± 0.050	−30.57 ± 8.63	−2.17 ± 8.63
8:35:32.57	+17:06:30.9	–	19.562 ± 0.105	18.436 ± 0.064	17.852 ± 0.073	17.193 ± 0.071	17.160 ± 0.047	−14.73 ± 6.72	−18.78 ± 6.72
8:33:42.21	+18:47:10.3	–	19.784 ± 0.110	18.427 ± 0.066	17.615 ± 0.061	17.015 ± 0.064	17.029 ± 0.039	−33.11 ± 6.29	−9.67 ± 6.29
8:47:13.71	+18:16:38.3	–	–	18.693 ± 0.119	17.675 ± 0.060	16.954 ± 0.064	16.967 ± 0.041	−40.67 ± 9.93	6.83 ± 9.93
8:43:52.01[a]	+17:39:20.7[a]	–	–	18.552 ± 0.091	17.894 ± 0.066	17.178 ± 0.063	17.203 ± 0.044	−19.91 ± 9.48	−17.76 ± 9.48

[a] A visual inspection of the *ZYJHK*1*K*2 images suggests a possible companion.

Table 5. A table containing the fitted parameters for each magnitude range. For definitions of each term see Deacon & Hambly (2004). Note that in this case we did not freely fit the cluster proper motion standard deviation σ. Instead, this was calculated from the mean proper motion error in each magnitude bin.

Z range	N_{stars}	f	σ	μ_{xc}	μ_{yc}	τ	Σ_x	μ_{xf}
12–13	272	0.821	3.42	−2.03	35.63	13.97	17.01	−4.60
13–14	537	0.743	3.40	−2.55	35.24	16.67	16.95	−7.73
14–15	866	0.778	3.41	−2.31	35.04	14.89	16.64	−6.41
15–16	1146	0.823	3.40	−2.31	35.00	13.78	16.66	−6.69
16–17	1251	0.844	3.48	−2.79	35.02	11.46	15.42	−6.81
17–18	906	0.936	3.67	−2.34	35.08	11.24	14.11	−6.50
18–19	587	0.936	4.37	−3.75	34.93	11.44	14.33	−5.96
19–20	316	0.850	6.04	−2.51	34.16	11.88	16.05	−6.19
20–21	241	0.863	9.02	−3.17	32.83	16.02	18.09	−4.58

Table 6. Praesepe member candidates identified to have membership probabilities calculated from proper motions greater than 0.5. The nomenclature, as used above to identify the objects in this table, is UGCS JHHMMSS.SS ± DDMMDD.D. Table 6 is published in its entirety as supporting information with the electronic version of the journal. A fraction is shown here for guidance regarding its form and content.

Name	Membership probability	Z	Y	J	H	K
UGCS J084344.72+211234.2	0.85	12.996 ± 0.001	12.710 ± 0.001	12.203 ± 0.001	11.615 ± 0.001	11.360 ± 0.001
UGCS J084037.87+202017.9	0.92	12.865 ± 0.001	12.614 ± 0.001	12.169 ± 0.001	11.607 ± 0.001	11.379 ± 0.001
...	...	...	...	...	...	...
UGCS J083814.20+194723.4	0.83	12.464 ± 0.002	12.189 ± 0.001	11.744 ± 0.001	11.500 ± 0.001	10.942 ± 0.001
UGCS J083829.61+195145.0	0.82	12.195 ± 0.001	12.010 ± 0.001	11.695 ± 0.001	11.617 ± 0.001	10.918 ± 0.001

for candidates with masses below $0.15\,M_\odot$. Within $3°$ from the cluster centre, this gives a contamination of 11.9, 9.8 and 23.8 per cent for the same mass range, respectively, or 18.7 per cent for the whole Praesepe sample.

These numbers appear quite large. We stress again that these are upper limits, since the coverage is not complete at the tidal radius of Praesepe and beyond. However, we can claim completeness in our cluster candidate list, and MF determination, better than 90 per cent. This is justified by the fact that our astrometric selection includes all objects within 3σ of the cluster's mean proper motion (completeness of >99 per cent) and that the lines used in our photometric selection go at least 2σ bluer from the cluster main sequence in all the CMD used for the photometric selection (completeness of $\sim$95.4 per cent).

In Fig. 8 (left-hand panel), we present the K versus $Z - K$ CMD of all GCS point sources towards Praesepe (small dots) and the cluster candidates based on our astrometric and photometric selections (larger dots). We observe three structures in this diagram. The structure at $Z - K \sim 0.6$ mag contains predominantly Galactic disc turn-off stars and the structure at $Z - K \sim 1.7$ mag represents Galactic disc late-type and giant stars, while the structure at $Z - K \sim 2.5$ mag is mostly composed of galaxies. This indicates that most of the contaminants of our cluster candidates with masses above $0.15\,M_\odot$ would be Galactic disc late-type and giant stars, while most of the contaminants of candidates less massive than $0.15\,M_\odot$ would not only include Galactic disc late-type and giant stars, but also unresolved galaxies.

6 DISCUSSION ON THE BINARY FREQUENCY

Here we investigate the multiplicity of low-mass and very low mass Praesepe members using the photometry and colours from the GCS.

We selected binary candidates in the following way. We used the Z versus $Z - K$ CMD (Fig. 9) to define three mass ranges: between 0.45 and $0.2\,M_\odot$, between 0.2 and $0.1\,M_\odot$ and between 0.1 and $0.07\,M_\odot$. These mass cuts were chosen as they can be compared directly with the binary fraction obtained from the hydrodynamical simulation by Bate (2012, with the mass intervals of 0.5–$0.2\,M_\odot$, 0.2–$0.1\,M_\odot$ and 0.1–$0.07\,M_\odot$)). At each transition of these mass ranges, we defined an area starting from 0.376 mag brighter to 1.13 mag fainter than the cluster sequences (single objects), and an area starting from 0.376 mag brighter to 1.5 mag brighter than the cluster main sequence (binary candidates). The binary fraction is the ratio between the number of objects in the brighter area, with the sum of both areas, for each mass range. Because of our 3σ selection in astrometry and $\sim$2.5σ bluer in photometry, we expect to be complete up to 97 per cent in our selection between the saturation and detection limit, bracketing the mass intervals used for the binary fraction estimation.

Our binary candidates are presented in a Z versus $Z - K$ CMD shown in Fig. 9. The binary fraction we obtain is 25.8 ± 3.7 per cent in the mass range 0.07–$0.1\,M_\odot$, 19.6 ± 3.8 per cent in 0.1–$0.2\,M_\odot$, and 23.3 ± 7.3 per cent in 0.2–$0.5\,M_\odot$. We present these binary fractions in Table 7, and we compare them directly with those obtained from the hydrodynamical simulation by Bate (2012),[2] and also the photometric determination by Pinfield et al. (2003).

We observe a similar binary fraction to Bate (2012) between 0.07 and $0.1\,M_\odot$ (within 1σ, where σ is the error on our measurements), a disagreement of only $\sim$1.5σ for the binary fraction in the mass range 0.2–0.45 $M_\odot$, but a significantly lower binary fraction by

[2] Table 2 from Bate (2012) presents the number of single objects, and also the number of binary, triple and quadruple systems per each mass range obtained from their hydrodynamical simulation. In our analysis, we only consider the binary system.
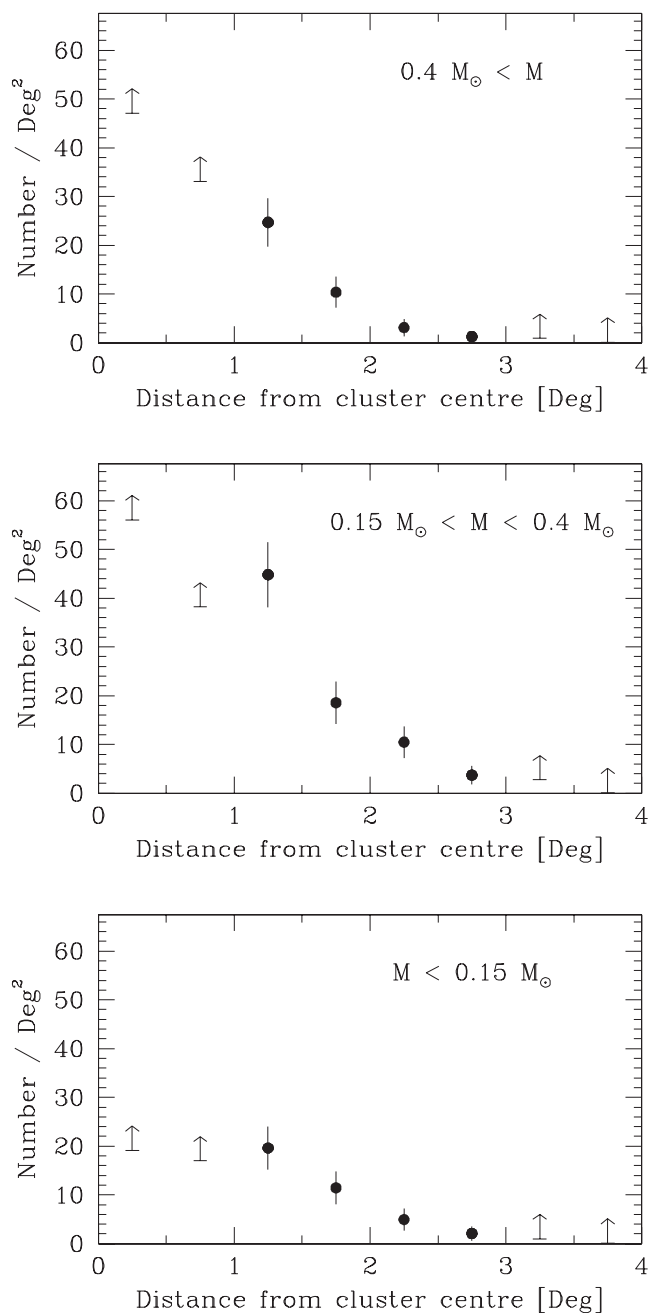
Figure 7. Radial density plots of our candidate members of Praesepe in three mass ranges: above $0.4\,M_\odot$ (top panel), between 0.15 and $0.4\,M_\odot$ (middle panel) and below $0.15\,M_\odot$ (bottom panel). The error bars at each data point are Poissonian arising from the number of objects in each bin. The arrows represent lower limits, as we are not complete in these bins.

more than 3σ for the mass range 0.1–$0.2\,M_\odot$. However, we note that the binary fraction in fig. 7 of Bate (2012) is also higher compared to previous observations of the binary fraction for field dwarfs below $0.2\,M_\odot$ (Close et al. 2003; Basri & Reiners 2006).

Our binary fraction is lower by $\sim 1.8\sigma$ than the value of Pinfield et al. (2003) for masses in the range 0.35–$0.6\,M_\odot$ (0.2–$0.45\,M_\odot$ for our work). On the other hand, their binary fraction for lower masses is significantly higher by a factor of 2 than our values (more than 4σ for the mass range 0.07–$0.1\,M_\odot$, and more than 8σ for the mass range 0.1–$0.2\,M_\odot$) and is also significantly higher than those of Bate (2012) (considering the error bars of Pinfield et al. 2003).

We attribute this overestimation of binary frequency to the selection method used by Pinfield et al. (2003). These authors used a method similar to the one used here, i.e. by defining an area above the cluster sequences corresponding to the binary population. However, they used a cluster sequence constructed both from isochrones and empirical data. The resulting assumed cluster sequence appears bluer than the observed cluster sequence by about $I - K \sim 0.2$ mag at $K \sim 14$ mag (see fig. 3 of Pinfield et al. 2003). This would give a *fainter* equal-mass binary sequence, and therefore, overestimate the number of binaries and the binary fraction.

Using the probabilistic analysis presented in Section 4.4, we obtain similar binary fractions using objects with a membership probability higher than 50 per cent, i.e. 27.9 per cent in the mass range 0.07–$0.1\,M_\odot$, 18.0 per cent in 0.1–$0.2\,M_\odot$, 26.6 per cent in 0.2–$0.5\,M_\odot$ and 23.7 per cent in the whole mass range from 0.07 to $0.5\,M_\odot$.

7 VARIABILITY AT 600 MYR

Here we discuss the variability of the Praesepe member candidates using the two epochs provided by the GCS in the K band ($K1$ being the first epoch, $K2$ the second).

In Fig. 10, we present the difference in the K magnitudes (i.e. $K1 - K2$) as a function of the K magnitude (average of $K1$ and $K2$) for all the photometric and astrometric candidates. The brightening observed at $K < 12$ mag is due to the difference in depth between the first and the second epoch, which causes a decrease of 0.5 mag in the completeness limit, but also in the saturation limit.[3] Therefore, objects with $K < 12$ mag are excluded from our variability analysis.

We selected as variable all objects with $|K1 - K2|$ larger than 3σ, where σ is the standard deviation of $K1 - K2$ around the K magnitude of the object. Nine objects are identified as variable candidates. We looked at the UKIDSS GCS DR9 $ZYJHK1K2$ images and give our comments in Table 8. One source has its photometry affected by the presence of a nearby object, while one other might show spurious variability due to poorer image quality in one of the K-band images. There are seven remaining objects which are likely to be variable objects in Praesepe, which is 0.63 per cent of our member candidates (black circles with dots in Fig. 10). One of the variable candidates, UGCS J084353.41+210126.3, is in the substellar regime with an estimated mass of $0.064 \pm 0.013\,M_\odot$.

Using the probabilistic analysis, we also obtain six objects with $|K1 - K2|$ larger than 3σ (0.59 per cent of the cluster candidate having a membership probability higher than 50 per cent, including three from the variable candidate sample from the astrometric and photometric selection).

8 LUMINOSITY AND MASS FUNCTION

8.1 Isochrone of Praesepe

We derived a NextGen isochrone using a grainless atmosphere and evolutionary tracks (Baraffe et al. 1998; Hauschildt, Allard & Baron 1999) and a DUSTY isochrone using a dusty atmosphere and evolutionary tracks (Chabrier et al. 2000; Allard et al. 2001). We used the known astrophysical parameters of Praesepe (age, distance) presented in Section 1 (and assumed solar metallicity as well as negligible reddening).

---

[3] The exposure times have been doubled for the second epoch with relaxed constraints on the seeing requirement and weather conditions.
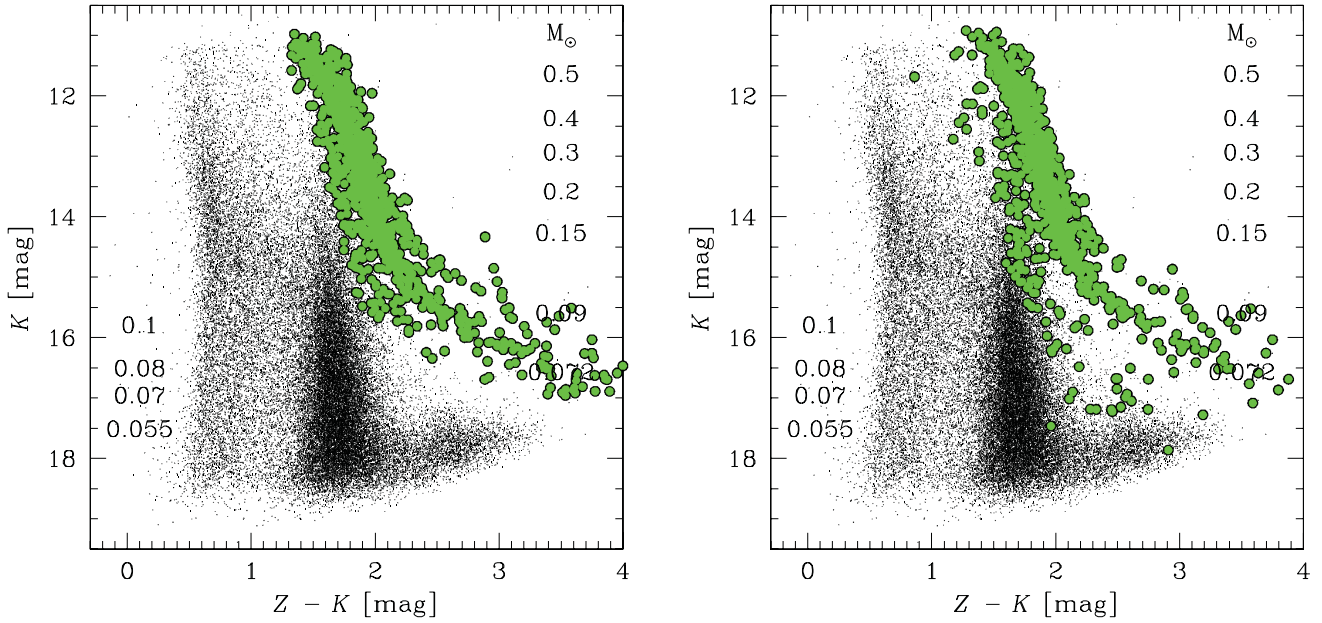
Figure 8. Left-hand panel: CMD of K versus $Z - K$ of all detected objects towards the Praesepe from the UKIDSS GCS DR9. For clarity, only one of five objects are plotted. We also show the objects which are recovered in our astrometric and photometric selection (larger green dots, see Section 4). The structure at $Z - K \sim 0.6$ mag contains predominantly Galactic disc turn-off stars and the structure at $Z - K \sim 1.7$ mag is Galactic disc late-type and giant stars, while the structure at $Z - K \sim 2.5$ mag is mostly composed of galaxies. The NextGen isochrone masses corresponding to the K magnitudes are on the right, while the DUSTY isochrone masses are on the left. Right-hand panel: same as the left-hand panel, but using the objects with a membership probability higher than 50 per cent from the probabilistic analysis.
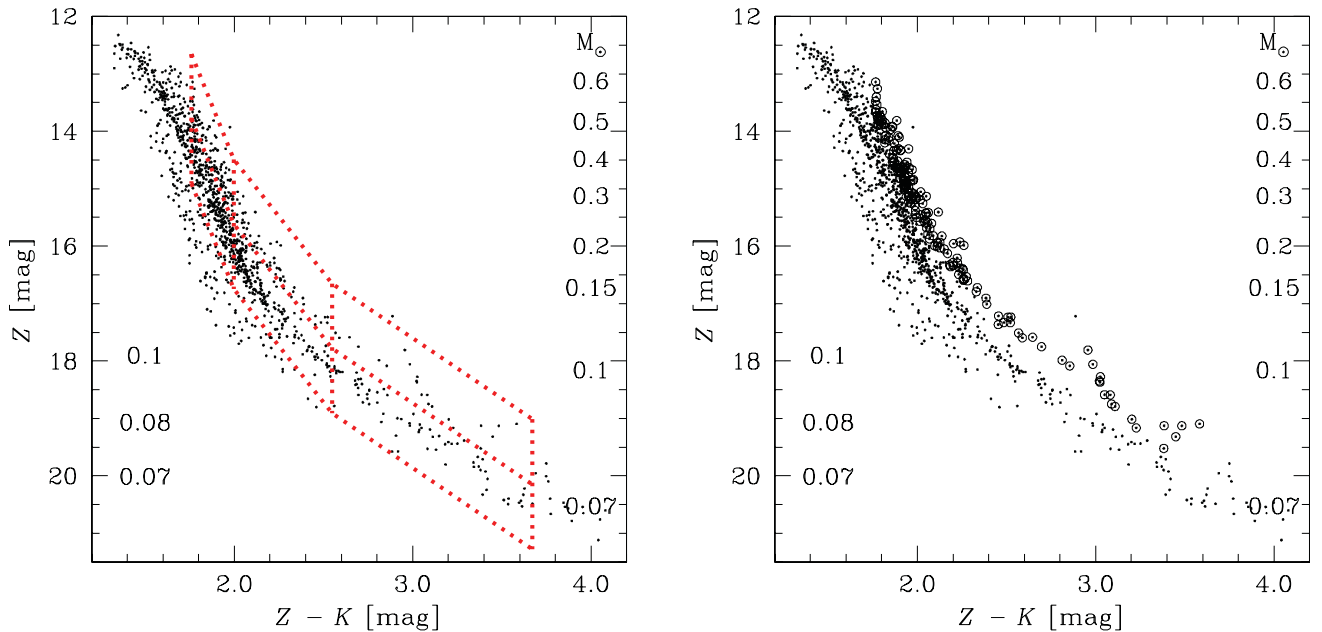
Figure 9. CMD of Z versus $Z - K$ of all our cluster candidates of Praesepe from the UKIDSS GCS DR9. The NextGen isochrone masses are on the right, while the DUSTY isochrone masses are on the left. Left-hand panel: the red dotted boxes show the selection areas for single objects (bottom) and for binaries (top). Right-hand panel: the dots are single objects and circles with dots are binary candidates with masses between 0.5 and 0.07 $M_\odot$.

The models and assumptions provide us with a prediction of f_λ, the spectral energy distribution (SED) received at the Earth (in erg cm^{-2} s^{-1} Å^{-1}) from the source. We need to convert these spectra to magnitudes in the WFCAM filters $ZYJHK$. Denoting as $S_A(\lambda)$ the (known) total transmission function of filter A (including the CCD quantum efficiency and assuming telescope and instrumental

throughput is flat), then the flux measured in the filter is

$$f_A = \frac{\int_0^\infty f_\lambda S_A(\lambda)\, d\lambda}{\int_0^\infty S_A(\lambda)\, d\lambda}. \tag{7}$$

The corresponding magnitude m_A in the Johnson photometric system is given by

Table 7. Binary fraction from our work on Praesepe compared to the simulation of Bate (2012). Errors on the fractions are Poissonian arising from the number of single objects and the number of binary candidates. We also give the binary fraction observed by Pinfield et al. (2003). Numbers obtained using the probabilistic analysis are in parentheses.

Mass range ($M_\odot$)	Single	Binary	Per cent	Bate
0.07–0.1	73 (44)	22 (17)	23.2 ± 5.6 (27.9)	27.3 ± 11.6
0.1–0.2	225 (201)	55 (44)	19.6 ± 3.0 (18.0)	29.2 ± 5.3
0.2–0.45	279 (256)	96 (91)	25.6 ± 3.0 (26.2)	32.1 ± 4.7^a
0.07–0.45	588 (538)	176 (167)	23.1 ± 2.0 (23.3)	29.2 ± 2.0
Pinfield et al.				
0.09–0.11	–	–	47^{+13}_{-11}	–
0.2–0.35	–	–	44 ± 6	–
0.35–0.6	–	–	31^{+7}_{-6}	–

^{a}Bate (2012) used the interval 0.2–0.5 $M_\odot$, but the values presented here are for the interval 0.2–0.45 $M_\odot$ (Bate 2012 private communication).
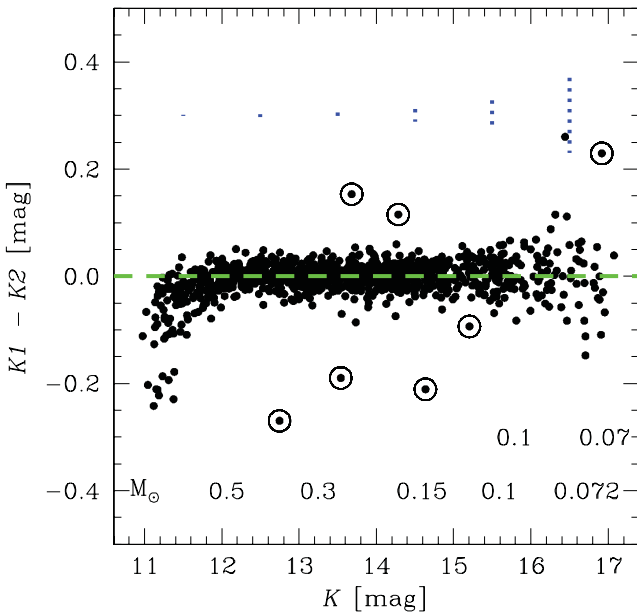
Figure 10. Difference in the K magnitude (i.e. $K1 - K2$) as a function of the K magnitude (average of $K1$ and $K2$) for all the photometric and astrometric candidates (*black dots*). The error bars on $K1 - K2$ are given as *blue* vertical lines, while the horizontal *green* line marks zero. The variable candidates from our Praesepe cluster candidate list are presented as black circles with dots. At the bottom of the figure, the NextGen isochrone masses are at the bottom while the DUSTY isochrone masses are above.

$$m_A = -2.5 \log f_A + c_A, \tag{8}$$

where c_A is a constant (zero-point) that remains to be determined in order to put the model-predicted magnitude on to the Johnson system. We determine this constant for each of the UKIDSS $ZYJHK$ bands in the standard way, namely by requiring that the spectrum of Vega produce a magnitude, m_A, of 0.03 mag in V and zero for all colours in all bands. Using the Vega spectrum from Colina, Bohlin & Castelli (1996), the zero-point constants we obtain for the UKIDSS $ZYJHK$ bands are $c_Z = -22.6587$, $c_Y = -23.1075$, $c_J = -23.8080$, $c_H = -24.8365$ and $c_K = -26.0014$ mag. Applying equations (8) and (9) to the model spectra produces a theoretical isochrone in colour–magnitude space.

Unlike most of the open cluster surveys that use one magnitude or one colour to estimate masses and effective temperatures ($T_{\rm eff}$), here we take full advantages of the five bands available (i.e. $ZYJHK$) by determining the masses and $T_{\rm eff}$ for each object from its SED as in Boudreault & Bailer-Jones (2009, using a least-squares fit between the measured SED and the model SED from the isochrone) with normalization at J.[4] See Fig. 11 for an illustrative example of the resulting fitting for three cluster candidates at three different masses.

The errors on the derived physical parameters (i.e. on mass and $T_{\rm eff}$) take into account the errors on the derived age of the cluster and the errors on the fitting.

8.2 The cluster luminosity function

In Fig. 12, we present the LF of Praesepe using the Z- and J-band photometry of our final list of candidates presented in Section 4. Magnitude bins are 0.5 mag wide for both LFs. We observe a rise in the LF, a turnover (at $Z \sim 16$ mag and $J \sim 15$ mag), followed by a decrease to lower magnitudes. The turnover in the J-band LF is at 1 mag brighter than observed with the cluster candidates from Boudreault et al. (2010), based on their NextGen pure photometric selection.

The overall shape of the LF, including the position of the turnover, remains unchanged with the binning (binning moved by 0.25 mag, bin size increased or decreased by a factor of 2).

8.3 The cluster mass function

The MF, $\xi(\log_{10}M)$, is generally defined as the number of stars per cubic parsec in the logarithmic mass interval $\log_{10}M$ to $\log_{10}M + {\rm d}\log_{10}M$ (Salpeter 1955). Here, we define the MF as the total number of objects in each $0.1\log_{10}M$ bin per square degree. Since we do not make any corrections for binaries, we compute here a system MF. This decision was taken considering that the binary fraction we have estimated in Section 6 does not cover the whole mass range of the MF (and therefore, only a few mass bins could be corrected) and also considering that all other MFs used in our analysis in Section 8.3 are also system MFs. However, an MF with the mass interval 0.45–0.07 $M_\odot$ corrected for binarity is presented at the end of this section.

We present the MF of Praesepe in Fig. 13 and the number of objects in each mass bin in Table 9. We observe that the MF has a maximum at $\sim 0.6\,M_\odot$ and then decreases to lower masses. We also note that our determination of the MF is unique in the sense that all previous determinations of the MF of Praesepe show an increase from 1 to $0.1\,M_\odot$ (Fig. 14). Previous studies include surveys based on photometry (e.g. Chappelle et al. 2005; Boudreault et al. 2010) and astrometry (e.g. Hambly et al. 1995; Kraus & Hillenbrand 2007).

One possible explanation is the coverage of our survey, i.e. the lack of completeness in the core (i.e. within 1°.1 from the cluster centre). However, considering that the most massive objects should be in the cluster's core, a full coverage would rather increase the observed slope in our MF of Praesepe. To rule out this possibility, we compared the MF of Praesepe within 1°.25, and beyond 1°.25 (Fig. 15), where 1°.25 corresponds to the half-mass radius of Praesepe (Adams et al. 2002). We can see that in both regions of the cluster, the MF decreases towards lower masses.

---

[4] We looked at the minimized sum of the square of the residuals as a function of the effective temperature, and there is no general trend for a better fit to higher or lower temperature.

Table 8. Seven Praesepe member candidates identified as likely variables, with two doubtful candidates. We give RA, Dec., K, $K1 - K2$, and comment on each object after visual inspection of the UKIDSS GCS DR9 $ZYJHK1K2$ images.

RA (^{h} ^{m} ^{s})	Dec. (° ′ ″)	K (mag)	$K1 - K2$ (mag)	Comments
8:48:45.42	+22:23:37.2	14.636 ± 0.012	-0.211	–
8:49:10.96	+22:12:13.2	13.681 ± 0.006	0.153	–
8:38:07.18	+21:16:36.8	14.284 ± 0.006	0.115	–
8:43:53.41	+21:01:26.3	16.918 ± 0.066	0.229	–
8:36:45.00	+20:08:45.8	13.734 ± 0.005	-0.086	Faint object observed nearby. Possible companion.
8:50:49.83	+19:48:36.5	12.747 ± 0.002	-0.270	–
8:41:24.84	+19:57:27.0	15.205 ± 0.018	-0.093	–
8:35:13.24	+17:02:06.5	13.540 ± 0.004	-0.190	–
8:41:50.08	+19:06:18.3	16.443 ± 0.052	0.260	White dots on the object are $K1$ images (i.e. bad pixels or cosmics).
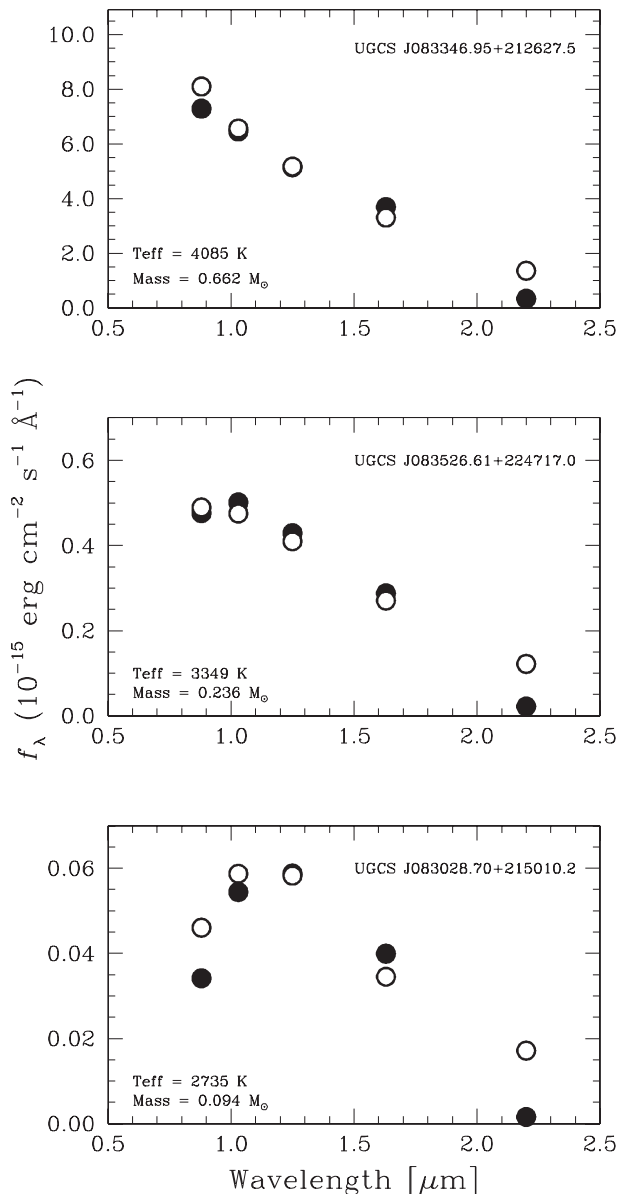
Figure 11. Fitting of the SED for three cluster candidates in our sample. The open circles are the flux measurements from the $ZYJHK$ UKIDSS magnitudes, while the filled circles are the least-squares fit obtained using the isochrones. The values of masses and $T_{\rm eff}$ are given in each panel, as well as their name following the IAU nomenclature (see Table 2).
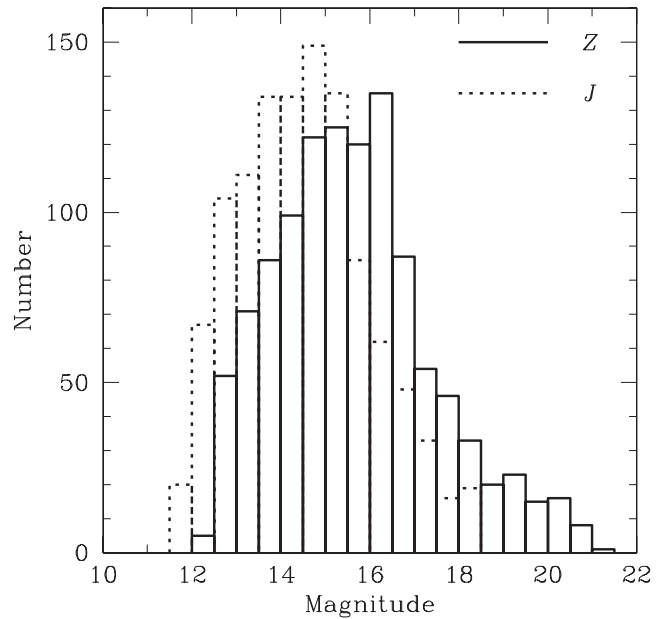
Figure 12. LF of Praesepe using the Z (solid line) and J (dotted line) band photometry of our final list of $ZYJHK$ member candidates. Magnitude bins are 0.5 mag wide for both LFs.

Incompleteness can also be ruled out as an explanation for the discrepancy observed. As can be seen in Fig. 13, the completeness limit and the saturation limit are affecting the lowest mass bin and the highest mass bin only. The incompleteness, alone, cannot explain the overall shape of the MF.

One could question the mass determination or the selection methods as a possible source of discrepancy. However, considering that we use the same mass-determination method as from Boudreault et al. (2010), and we use a similar filter set and a similar selection method as in Baker et al. (2010),[5] such an explanation seems unlikely.

However, we emphasize that we can reproduce the shape of previous determinations of the MF if we remove the selection based on astrometry. This is presented in Fig. 16, where we show our determination of the MF of the Praesepe, both with and without the astrometric selection. We can see that the difference between the two MFs goes from -0.1 dex at $0.5\,{\rm M}_\odot$ to $+0.3$ dex at $0.1\,{\rm M}_\odot$.

---

[5] Baker et al. (2010) combined the UKIDSS DR6 with 2MASS and the Sloan Digital Sky Survey.
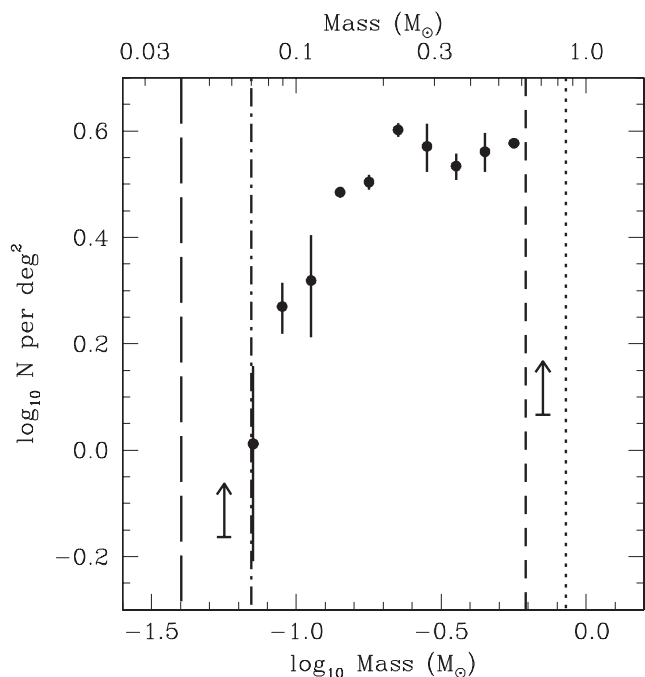
Figure 13. The Praesepe MF. The error bars are obtained using the errors on the age of Praesepe. The vertical long dashed line is the lowest completeness limit (at $K2 = 18.4$ mag, $M = 0.04\,M_\odot$). The vertical dash–dotted line is the highest completeness limit (at $Z = 20.4$ mag, $M = 0.07\,M_\odot$). The vertical short dashed line is the lowest saturation limit (at $H = 11.4$ mag, $M = 0.62\,M_\odot$). The vertical dotted line is the highest saturation limit (at $J = 10.9$ mag or $M = 0.85\,M_\odot$). The arrows represent lower limits, as we are not complete in these mass bins.

Table 9. Number of objects in each mass bin.

M ($M_\odot$)	$\log_{10} M$ ($M_\odot$)	N (pc^{-3})	$\log_{10} N$ (pc^{-3})
0.056	−1.25	2[a]	−0.163[a]
0.071	−1.15	37 ± 15	$0.012^{+0.146}_{-0.221}$
0.089	−1.05	67 ± 7	$0.270^{+0.045}_{-0.050}$
0.112	−0.95	75 ± 16	$0.319^{+0.085}_{-0.106}$
0.142	−0.85	110 ± 2	0.485 ± 0.010
0.178	−0.75	115 ± 4	0.504 ± 0.014
0.224	−0.65	144 ± 4	0.602 ± 0.013
0.282	−0.55	134 ± 14	$0.571^{+0.043}_{-0.048}$
0.356	−0.45	123 ± 7	$0.534^{+0.024}_{-0.026}$
0.448	−0.35	131 ± 11	$0.561^{+0.035}_{-0.038}$
0.564	−0.25	136 ± 1	$0.577^{+0.004}_{-0.005}$
0.710	−0.15	42[a]	0.067[a]

[a]Lower limits.

The MF we obtain for the Praesepe without astrometric selection is also very similar to the one obtained by Chappelle et al. (2005), with an increase of the MF of ∼0.2 dex from 0.5 down to 0.1 $M_\odot$.

We therefore conclude that our determination of the Praesepe MF is different to the previous work due to our selection based on astrometry *and* photometry, which includes five filters covering the SED from 0.85 to 2.3 μm. Surveys based only on photometry would appear to suffer from contamination by field M dwarfs and background red giants (e.g. Chappelle et al. 2005; Boudreault et al. 2010).
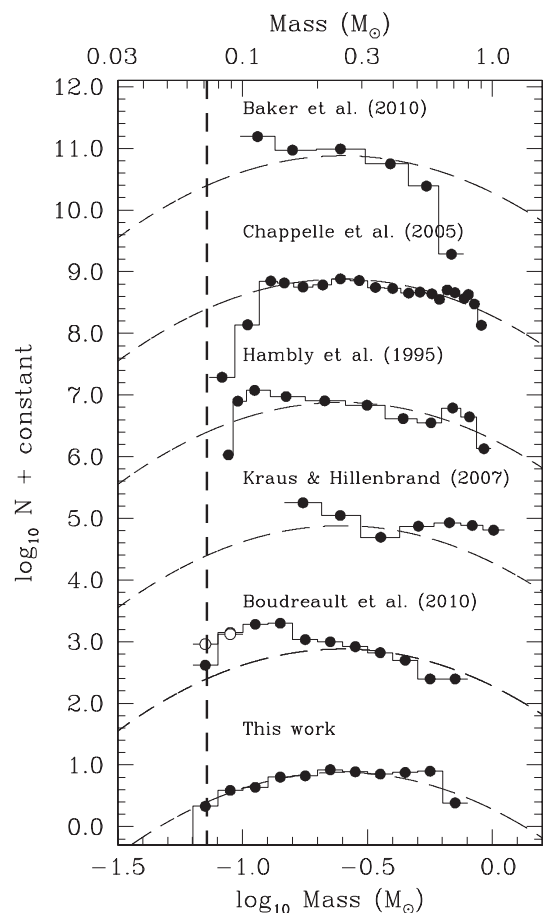
Figure 14. MFs of Praesepe from our present work and from previous work. We also show the system Galactic field star MF from Chabrier (2005) as the dotted curved lines and the substellar limit as a vertical dashed line. We normalized all the MFs to the log-normal fit of Chabrier (2005) at ∼0.3 $M_\odot$ ($\log M \sim -0.5$).

As for the work of Kraus & Hillenbrand (2007), the overall shape of the MF presents a rise of 0.4 dex from 1 down to 0.2 $M_\odot$. However, one needs to be careful with the lowest bin because this survey is ∼70 per cent complete at M5 dwarfs (corresponding to 0.15–0.2 $M_\odot$ in Praesepe).

It could be suggested that a larger spatial coverage should in principle detect a larger fraction of low-mass stars due to mass segregation. However, our spatial coverage is larger than the survey of Baker et al. (2010) and Hambly et al. (1995), and we obtain a larger ratio of the number of intermediate-mass stars to lower-mass stars. Mass segregation does not appear to be the cause of the discrepancy in the MF in the low-mass star regime.

We compare our determination of the MF of Praesepe with the Hyades open cluster in Fig. 17, which has a similar age of ∼600 Myr (Bouvier et al. 2008). We see now that both clusters present a decreasing MF to lower masses, unlike what was previously reported (Boudreault et al. 2010). However, the Praesepe remains different to the Hyades MF, with a decreasing MF of only ∼0.2 dex from 0.6 down to 0.1 $M_\odot$, compared to ∼1 dex for the Hyades.

In Fig. 18, we present the MF of α Per (85 ± 5 Myr; Lodieu et al. in preparation) and the Pleiades (125 ± 8 Myr; Lodieu et al. 2012) open clusters, compared with the MF of Praesepe. The α Per and Pleiades MFs are obtained using the same survey and selection procedure as our current work on the Praesepe, i.e. using the *ZYJHK*
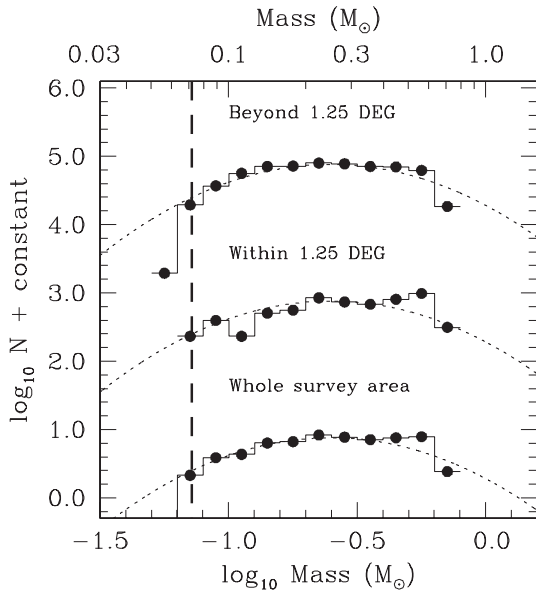
Figure 15. MF of Praesepe for the whole survey area compared to the MF of Praesepe within 1°.25 of the cluster centre and beyond 1°.25 from the cluster centre. The dotted curved lines, the vertical dashed line and the normalization of all the MFs at ∼0.3 M$_\odot$ are the same as in Fig. 14.
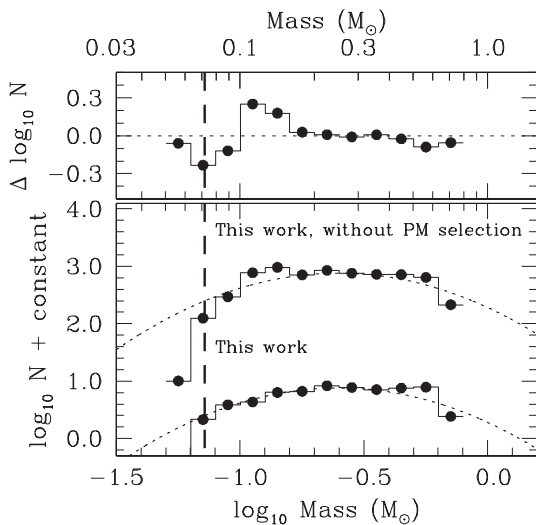

Figure 16. MF of Praesepe from our present work with astrometric and photometric selections (bottom) and without selection based on proper motion (PM, top). The dotted curved lines, the vertical dashed line and the normalization of all the MFs at ∼0.3 M$_\odot$ are the same as in Fig. 14. We also show in the top panel of the figure the difference between the two MFs.

photometry and astrometric data from UKIDSS GCS DR9. We observe that the MF of Praesepe in the mass range 0.072–0.6 M$_\odot$ is more similar to the MF of α Per than the MF of the Pleiades. This is surprising as dynamical evolution would give an MF with a shape more similar to or in between the shape of the MF of the Pleiades and the Hyades, which are clusters with, respectively, ages of ∼125 (Stauffer, Schultz & Kirkpatrick 1998) and ∼600 Myr. These values are closer to the age of Praesepe ($\tau = 590^{+150}_{-120}$ Myr; Fossati et al. 2008), compared to α Per (85 ± 5 Myr; Barrado y Navascués, Stauffer & Jayawardhana 2004).
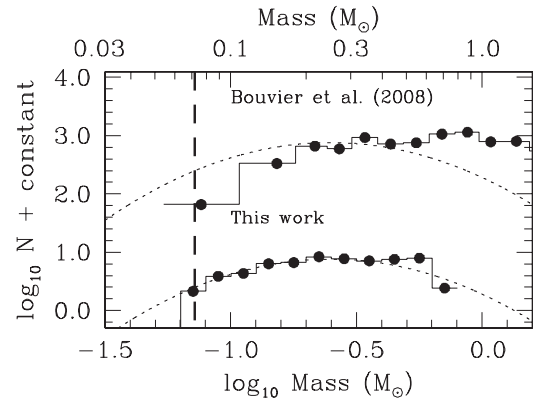
Figure 17. MF of Praesepe from our present work compared with the MF of the Hyades from Bouvier et al. (2008). The dotted curved lines, the vertical dashed line and the normalization of all the MFs at ∼0.3 M$_\odot$ are the same as in Fig. 14.
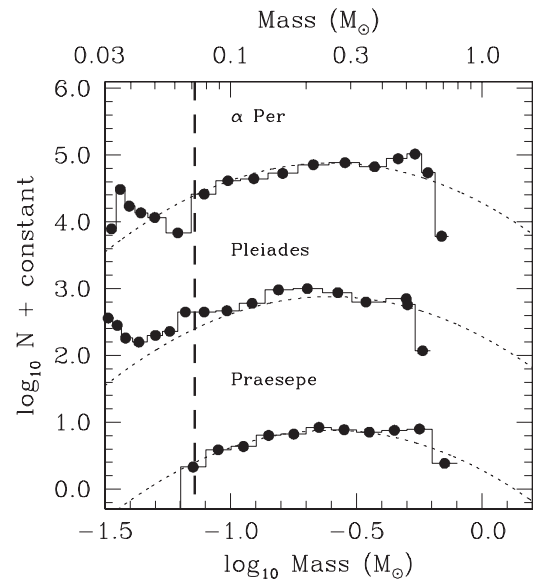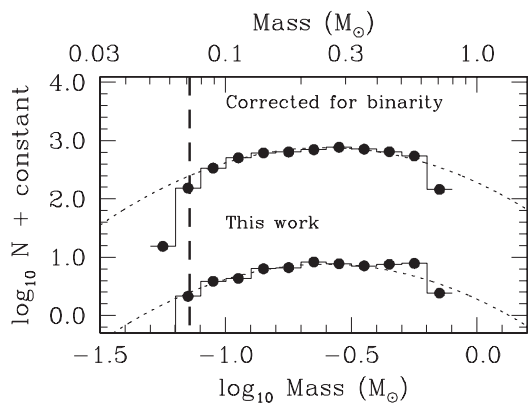

Figure 18. MFs of Praesepe, the Pleiades and α Per. The dotted curved lines, the vertical dashed line and the normalization of all the MFs at ∼0.3 M$_\odot$ are the same as in Fig. 14.

Finally, we present in Fig. 19, the MF of Praesepe from this work corrected for binarity (i.e. between 0.45 and 0.07 M$_\odot$). For this, we assume that all binary candidates in Fig. 9 have a mass ratio of 1.0 for each object. (With the photometry alone, it is not possible to make a reliable estimation of what would be the binary mass ratio.) The shape of the MF obtained is similar to the system MF, i.e. a decrease from 0.6 down to 0.1 M$_\odot$. However, we stress that this *single star* MF should be used with caution, considering our assumption about the binary mass ratio and the fact that binary candidates are not known for the *whole* mass range of our *system* MF.

9 SUMMARY AND CONCLUSIONS

In this paper, we presented the results of a wide-field, near-infrared study of the Praesepe cluster using the DR9 of the UKIDSS GCS. We performed an astrometric and photometric selection of 1116

Figure 19. MF of Praesepe including correction for binarity (top) and without correction (this work). The dotted curved lines, the vertical dashed line and the normalization of all the MFs at ∼0.3 M⊙ are the same as in Fig. 14.

cluster candidates out of the 218 141 point sources detected towards Praesepe.

Possible sources of contamination include Galactic disc late-type and giant stars and unresolved galaxies. We estimate a contamination of 11.9 per cent above 0.4 M⊙, 9.8 per cent in the mass range 0.15–0.4 M⊙ and 23.8 per cent below 0.15 M⊙.

We investigated the binary frequency of Praesepe using the photometry and colours from our cluster candidates. We observe a binary fraction similar to the simulation of Bate (2012) between 0.07 and 0.1 M⊙, ∼1.5σ difference in the 0.2–0.45 M⊙ mass interval and significantly lower by more than 3σ for the mass range 0.1–0.2 M⊙. On the other hand, the binary fractions from Pinfield et al. (2003) are higher than our values and those of Bate (2012). However, we note that two other works focusing on field low-mass stars have also derived binary fractions lower than Bate (2012).

We also studied the variability of the Praesepe candidates using the two K-band epochs provided by the GCS. We identified seven candidate variables, including one in the substellar regime.

We derived the LF of Praesepe in the Z and J bands here. We observed that the peak of the J-band LF is 1 mag brighter than the one reported by Boudreault et al. (2010).

Finally, we determined the MF of Praesepe, which differs from previous studies: while previous MFs showed an increase from 0.6 to 0.1 M⊙, our MF shows a decrease. We looked at the MF of Praesepe at two different regions of the cluster, i.e. within and beyond 1°.25, and we observed that both regions show an MF which decreases to lower masses. We compared our MF of Praesepe in the mass range 0.072–0.6 M⊙ with the ones of the Hyades, the Pleiades and α Per. We concluded that our MF of Praesepe is most similar to the MF of α Per although they are, respectively, of ages ∼85 and ∼600 Myr. Even though of similar age, the Praesepe appears different to the Hyades, with a decrease in the MF of only ∼0.2 dex from 0.6 down to 0.1 M⊙, compared to ∼1 dex for the Hyades.

ACKNOWLEDGMENTS

Casali et al. 2007). The photometric system is described in Hewett et al. (2006), and the calibration is described in Hodgkin et al. (2009). The pipeline processing and science archive are described in Irwin et al. (in preparation) and Hambly et al. (2008), respectively. We thank our colleagues at the UK Astronomy Technology Centre, the Joint Astronomy Centre in Hawaii, the Cambridge Astronomical Survey and Edinburgh Wide Field Astronomy Units for building and operating WFCAM and its associated data flow system. This research has made use of the SIMBAD data base, operated at the Centre de Données Astronomiques de Strasbourg (CDS), and of NASA's Astrophysics Data System Bibliographic Services (ADS).

REFERENCES

Adams J. D., Stauffer J. R., Skrutskie M. F., Monet D. G., Portegies Zwart S. F., Janes K. A., Beichman C A., 2002, AJ, 124, 1570
Allard F., Hauschildt P. H., Alexander D. R., Tamanai A., Schweitzer A., 2001, ApJ, 556, 357
Baker D. E. A., Jameson R. F., Casewell S. L., Lodieu N., Hambly N., 2010, MNRAS, 408, 2457
Baraffe I., Chabrier G., Allard F., Hauschildt P. H., 1998, A&A, 337, 403
Barrado y Navascués D., Stauffer J. R., Jayawardhana R., 2004, ApJ, 614, 386
Basri G., Reiners A., 2006, AJ, 132, 663
Bastian N., Covey K. R., Meyer M. R., 2010, ARA&A, 48, 339
Bate M. R., 2011, MNRAS, 419, 3115
Béjar V. J. S., Zapatero Osorio M. R., Rebolo R., Caballero J. A., Barrado D., Martín E. L., Mundt R., Bailer-Jones C. A. L., 2011, ApJ, 743, 64
Bihain G. et al., 2009, A&A, 506, 1169
Boudreault S., Bailer-Jones C. A. L., 2009, ApJ, 706, 1484
Boudreault S., Bailer-Jones C. A. L., Goldman B., Henning T., Caballero J. A., 2010, A&A, 510, 27
Bouvier J. et al., 2008, A&A, 481, 661
Casali M. et al., 2007, A&A, 467, 777
Chabrier G., 2003, PASP, 115, 763
Chabrier G., 2005, in Corbelli E., Palla F., Zinnecker H., eds, Astrophys. Space Sci. Library Vol. 327, The Initial Mass Function 50 Years Later. Springer, Dordrecht, p. 41
Chabrier G., Baraffe I., Allard F., Hauschildt P., 2000, ApJ, 542, 464
Chappelle R. J., Pinfield D. J., Steele I. A., Dobbie P. D., Magazzù A., 2005, MNRAS, 361, 1323
Close L. M., Siegler N., Freed M., Biller B., 2003, ApJ, 587, 407
Colina L., Bohlin R., Castelli F., 1996, Instrument Science Report CAL/SCS, 8, 1
Collins R. S., Hambly N. C., 2012, in Ballester P., Egret D., eds, in ASP Conf. Ser. Vol., Astronomical Data Analysis Software and Systems XXI. Astron. Soc. Pac., San Francisco, in press
Covey K. R., Bastian N., Meyer M. R., 2011, in Alfaro Navarro E. J., Gallego Calvente A. T., Zapatero Osorio M. R., eds, Stellar Clusters & Associations: a RIA Workshop on GAIA.
Cutri R. M. et al., 2003, 2MASS All Sky Catalog of Point Sources. The IRSA 2MASS All-Sky Point Source Catalog, NASA/IPAC Infrared Science Archive. http://irsa.ipac.caltech.edu/applications/Gator/
Deacon N. R., Hambly N. C., 2004, A&A, 416, 125
Fossati L., Bagnulo S., Landstreet J., Wade G., Kochukhov O., Monier R., Weiss W., Gebran M., 2008, A&A, 483, 891
Friel E. D., Boesgaard A. M., 1992, ApJ, 387, 170
González-García B. M., Zapatero Osorio M. R., Béjar V. J. S., Bihain G., Barrado Y Navascués D., Caballero J. A., Morales-Calderón M., 2006, A&A, 460, 799
Hambly N. C., Steele I. A., Hawkins M. R. S., Jameson R. F., 1995, A&AS, 109, 29
Hambly N. C. et al., 2008, MNRAS, 384, 637
Hauschildt P. H., Allard F., Baron E., 1999, ApJ, 512, 377

Hewett P. C., Warren S. J., Leggett S. K., Hodgkin S. T., 2006, MNRAS, 367, 454

Hodgkin S. T., Pinfield D. J., Jameson R. F., Steele I. A., Cossburn M. R., Hambly N. C., 1999, MNRAS, 310, 87

Hodgkin S. T., Irwin M. J., Hewett P. C., Warren S. J., 2009, MNRAS, 394, 675

Jeffries R. D., Naylor T., Devey C. R., Totten E. J., 2004, MNRAS, 351, 1401

Jones B. F., Cudworth K., 1983, AJ, 88, 215

Kraus A. L., Hillenbrand L. A., 2007, AJ, 134, 2340

Kroupa P., 2002, Sci, 295, 82

Kumar M. S. N., Schmeja S., 2007, A&A, 471, 33

Lawrence A. et al., 2007, MNRAS, 379, 1599

Leigh N., Umbreit S., Sills A., Knigge C., de Marchi G., Glebbeek E., Sarajedini A., 2012, MNRAS, 422, 1592

Lodieu N., Dobbie P. D., Deacon N. R., Hodgkin S. T., Hambly N. C., Jameson R. F., 2007, MNRAS, 380, 712

Lodieu N., Hambly N. C., Jameson R. F., Hodgkin S. T., 2008, MNRAS, 383, 1385

Lodieu N., Dobbie P. D., Deacon N. R., Venemans B. P., Durant M., 2009, MNRAS, 395, 1631

Lodieu N., Deacon N. R., Hambly N. C., 2012, MNRAS, preprint (arXiv:1204.2659v1)

Lucas P. W. et al., 2010, MNRAS, 408, 56

Marks M., Kroupa P., 2012, A&A, 543, 8

Myers A. T., Krumholz M. R., Klein R. I., McKee C. F., 2011, ApJ, 735, 49

Pace G., Pasquini L., Franois P., 2008, A&A, 489, 403

Peña Ramírez K., Zapatero Osorio M. R., Béjar V. J. S., Rebolo R., Bihain G., 2011, A&A, 532, 42

Pinfield D. J., Dobbie P. D., Jameson R. F., Steele I. A., Jones H. R. A., Katsiyannis A. C., 2003, MNRAS, 342, 1241

Quanz S. P., Goldman B., Henning T., Brandner W., Burrows A., Hofstetter L. W., 2010, ApJ, 708, 770

Salpeter E. E., 1955, ApJ, 121, 161

Sanders W. L., 1971, A&A, 14, 226

Skrutskie M. F. et al., 2006, AJ, 131, 1163

Stauffer J. R., Schultz G., Kirkpatrick J. D., 1998, ApJ, 499L, 199

Taylor B. J., 2006, AJ, 132, 2453

van Leeuwen F., 2009, A&A, 497, 209

Wang W., Boudreault S., Goldman B., Henning Th., Caballero J. A., Bailer-Jones C. A. L., 2011, A&A, 531, 164

SUPPORTING INFORMATION

Additional Supporting Information may be found in the online version of this article:

Table 2. Praesepe member candidates based on our astrometric and photometric selection. Here we present the photometry and the astrometry of the candidates.

Table 3. Praesepe member candidates based on our astrometric and photometric selection. Here we present the physical parameters of the candidates, i.e. mass and effective temperature.

Table 6. Praesepe member candidates identified to have membership probabilities calculated from proper motions greater than 0.5.

Please note: Wiley-Blackwell are not responsible for the content or functionality of any supporting materials supplied by the authors. Any queries (other than missing material) should be directed to the corresponding author for the article.

This paper has been typeset from a TEX/LATEX file prepared by the author.